The Fundamental Solution of the Time-Dependent System of Crystal Optics.

Robert Burridge
Earth Resources Laboratory
Massachusetts Institute of Technology
42 Carleton Street, E34-450
Cambridge, MA 02142-1324

Jianliang Qian
Department of Mathematics
University of California, Los Angeles
405 Hilgard Avenue
Los Angeles, CA 90095-1555

February 1, 2004

Abstract

We set up the electromagnetic system and its plane-wave solutions with the associated slowness and wave surfaces. We treat the Cauchy initial-value problem for the electric vector and make explicit the quantities necessary for numerical evaluation. We use the Herglotz-Petrovskii representation as an integral around loops which, for each position and time form the intersection of a plane in the space of slownesses with the slowness surface. The field, especially its singularities, is strongly dependent on the varying geometry of these loops. We give without derivation the static term corresponding to the mode with zero wave speed. Numerical evaluation of the solution is presented graphically followed by some concluding remarks.

1 Introduction

1.1 General introduction

Crystal optics is similar to, but simpler than, anisotropic elasticity. For instance its slowness surface has conical points, in common with many elasticity systems, and there are conical points on the wave surface. It also has a third interesting feature associated with the rôle of the divergence in relation to Maxwell's equations, namely the fact that one characteristic speed is zero (actually two coincident zeros), so that the slowness surface is quartic rather than sextic as might be expected from the dimensionality - one quadratic sheet of the slowness surface lies at infinity. Remarkably the wave surface is another quartic surface of the same algebraic type, but with reciprocal parameters. See for instance Born and Wolf (1989) for a very full and readable account of the plane-wave theory of this system and the associated geometry.

The system of crystal optics is of great intrinsic and historical interest, the latter because Hamilton's prediction in 1833 of internal conical refraction, and Lloyd's experimental confirmation closely thereafter, led to the wide acceptance of Fresnel's wave theory of light. The intrinsic interest is largely centered around the remarkable geometrical properties of the slowness surface and wave surface, which are both of a type known as Fresnel's wave surface (Salmon, 1915).

We illustrate numerically the analytic expression for the fundamental solution of the system in terms of real loop integrals according to the Herglotz-Petrovskii formula, which may also be applied readily to other constant-coefficient hyperbolic systems. Petrowskii (1945) expressed the solution in terms of non-real cycles in complex space. Atiyah, Bott, and Garding (1970, 1973) placed Petrovskii's work on a modern basis, and De Hoop and Smit (1995) recently elaborated this in a three-dimensional elastodynamic setting. But following John (1955) and Gelfand and Shilov (1964) we will stay with the representation in terms of real integrals. Burridge (1967) used it to obtain the geometrical arrivals (see below), and the singularity due to the conical points of the slowness surface at field points in the interior of the cone of internal conical refraction for cubic elastic media. But that work lacked numerical illustrations and the treatment of the conical point was not uniform near the conical surface itself. Although we still do not give the uniform time-dependent asymptotic analysis for this region, we do present numerical solutions close to and on this 'cone of internal conical refraction'. The geometrical arrivals mentioned above are singularities in the field associated with slownesses $\boldsymbol{\xi}$ which are 'stationary points' where the plane $\boldsymbol{\xi}\cdot\boldsymbol{x} = t$ touches the slowness surface and at which the slowness surface has finite non-zero Gaussian curvature, and such wave arrivals are governed by the simplest form of geometrical ray theory.

For instance Movskin et al. (1993) have derived the Green's function in the frequency domain and discussed various important directions and cones of directions in relation to the field, namely in the directions of generators of the cone of internal conical refraction, and in the directions of the biradials, i.e. the directions of the conical points on the wave surface, and they obtain asymptotic approximations to the field at large distances in the neighborhoods of these directions.

In this paper we study the second-order vector equation for $\boldsymbol{E}$ obtained by eliminating the other dependent variables from Maxwell's equations and the constitutive laws of crystal optics. This equation is like the second-order elastodynamic equation for particle displacement and may be obtained from that of isotropic infinitesimal elasticity by setting the Lamé constant $\lambda = -2$, and $\mu = 1$, so that $\lambda + 2\mu = 0$, and the density $\rho = \boldsymbol{\sigma}$ (see below).

See Every (1981) the effects of curvature of the slowness surface near crystal symmetry axes in cubic crystal acoustics, and Shuvalov and Every (1996) for more general symmetries.

1.2 Outline of this paper

In Section 2 we set up the electromagnetic system and its plane-wave solutions with the associated geometrical entities such as the slowness surface, and the wave surface, and we show their remarkably tightly knit relationship to the energy ellipsoid and its parameterization by elliptic coordinates. In Section 3 we set up and solve the Cauchy initial-value problem for $\boldsymbol{E}$ and make explicit some quantities with a view to numerical evaluation. In Section 4 we follow the Herglotz-Petrovskii procedure of transforming the integral representation to an integral around loops which, for each $\boldsymbol{x}, t$, form the intersection of the plane $\boldsymbol{\xi}\cdot\boldsymbol{x} = t$ with the slowness surface. As $\boldsymbol{x}, t$ vary the geometry of these loops varies, and the field, especially its singularities, are strongly dependent on the geometry of these loops. In Section 5 we give without derivation the static term corresponding to the mode with zero wave speed. Numerical evaluation of the fundamental solution is presented graphically in Section 6 for a selection of points in the positive quadrant of the 13-plane. Section 7 contains some concluding remarks.

Table of notations:

Symbol	**Definition**
t.	time
$\boldsymbol{x} = (x_1, x_2, x_3)$	spatial coordinate vector.
$\boldsymbol{r} = (r_1, r_2, r_3)$	coordinate vector for the representation of $\mathcal{E}$.
c	the speed of light *in vacuo*.
$\boldsymbol{E}$, $\boldsymbol{H}$	the electric and magnetic vectors.
$\boldsymbol{D}$	The electric displacement.
$\boldsymbol{B}$	The magnetic induction.
μ	The magnetic permeability (scalar).

Symbol	Definition
$\boldsymbol{\epsilon}$	The dielectric tensor (symmetric).
$\boldsymbol{\sigma}$, σ_1, σ_2, σ_3	$\mu\boldsymbol{\epsilon}/c^2$ and its principal values.
$\boldsymbol{\xi}$	The slowness vector.
f	Plane wave pulse shape.
$\boldsymbol{e}$, $\boldsymbol{h}$, $\boldsymbol{d}$, $\boldsymbol{b}$	Constant polarization vectors for $\boldsymbol{E}$, $\boldsymbol{H}$, $\boldsymbol{D}$, $\boldsymbol{B}$, related to $\boldsymbol{\xi}$.
$\hat{\boldsymbol{x}}$	The unit vector in the direction of $\boldsymbol{x}$, and similarly for other vectors.
$\hat{\boldsymbol{x}}$, $\hat{\boldsymbol{y}}$, $\hat{\boldsymbol{z}}$, $\boldsymbol{x}^{\perp}$	Unit vectors (Section 5 and Appendix A only).
Ω, $\mathrm{d}\Omega$	The unit sphere and its surface element.
$\mathcal{E}$	The energy ellipsoid $\boldsymbol{r}^T\boldsymbol{\sigma}^{-1}\boldsymbol{r} = 1$.
u, v	Ellipsoidal coordinates on ellipsoid $\mathcal{E}$ $(\sigma_1 \geq u \geq \sigma_2 \geq v \geq \sigma_3 \geq 0.)$
$\mathcal{S}$, $\mathrm{d}S$	The slowness surface and its surface element.
$\boldsymbol{c}_{\mathcal{S}}$	A conical point on $\mathcal{S}$.
$\Pi_{\mathcal{S}}$	One of the four special tangent planes to $\mathcal{S}$.
$\mathcal{C}_{\mathcal{S}}$	One of the four circles in which a $\Pi_{\mathcal{S}}$ touches $\mathcal{S}$.
$\mathcal{W}$	The wave surface (reciprocal to $\mathcal{S}$).
$\boldsymbol{c}_{\mathcal{W}}$	A conical point on $\mathcal{W}$ (reciprocal to $\Pi_{\mathcal{S}}$).
$\Pi_{\mathcal{W}}$	One of the four special tangent planes to $\mathcal{W}$ (reciprocal to $\boldsymbol{c}_{\mathcal{S}}$).
$\mathcal{C}_{\mathcal{W}}$	One of the four circles in which $\Pi_{\mathcal{W}}$ touches $\mathcal{W}$.
$\mathcal{D}_{\mathcal{W}}$	The disk spanning $\mathcal{C}_{\mathcal{W}}$.
$\Sigma_{\pm}$, $\chi_{\pm}$	The two cones of internal conical refraction (vertex $\mathbf{0}$, base $\mathcal{C}_{\mathcal{W}}$), equation $\chi_{\pm}(\boldsymbol{x}) = 0$.
$\mathcal{L}$	Loop or loops forming the intersection of plane $\boldsymbol{\xi}\cdot\boldsymbol{x} = t$ with slowness surface $\mathcal{S}$.
$\boldsymbol{\nabla}$, $\dot{}$	Derivatives with respect to $\boldsymbol{x}$ and t.

Notes: 1) When used in matrix calculations vectors are columns unless explicitly transposed. (Thus $\boldsymbol{x}^T\boldsymbol{x}$ is a scalar and $\boldsymbol{x}\boldsymbol{x}^T$ is 3×3.) 2) There are four conical points $\boldsymbol{c}_{\mathcal{S}}$. $\boldsymbol{c}_{\mathcal{S}}$ in the singular refers to the $\boldsymbol{c}_{\mathcal{S}}$ in $\xi_1 > 0$, $\xi_3 > 0$. And similarly for some other quantities.

2 Crystal optics equations

2.1 Maxwell's equations and the slowness surface

We follow Born and Wolf (1991, Chapter XIV). Let $\boldsymbol{x} = (x_1, x_2, x_3) = (x, y, z)$ be cartesian coordinates and t the time. Maxwell's equations and the constitutive equations of crystal optics are

$$\begin{aligned} -\frac{1}{c}\dot{\boldsymbol{B}} &= \boldsymbol{\nabla} \times \boldsymbol{E}, & \frac{1}{c}\dot{\boldsymbol{D}} &= \boldsymbol{\nabla} \times \boldsymbol{H}, \\ \boldsymbol{B} &= \mu \boldsymbol{H}, & \boldsymbol{D} &= \boldsymbol{\epsilon} \boldsymbol{E}. \end{aligned} \tag{2.1}$$

Please refer to the Table of Notations for symbol definitions.

Since $\boldsymbol{E}$, $\boldsymbol{H}$, $\boldsymbol{D}$, and $\boldsymbol{B}$ may be expressed as superpositions of plane waves we shall seek them in a standard form for plane waves:

$$\begin{aligned} \boldsymbol{E} &= \boldsymbol{e}\, f(t - \boldsymbol{\xi}\cdot\boldsymbol{x}), & \boldsymbol{H} &= \boldsymbol{h}\, f(t - \boldsymbol{\xi}\cdot\boldsymbol{x}), \\ \boldsymbol{D} &= \boldsymbol{d}\, f(t - \boldsymbol{\xi}\cdot\boldsymbol{x}), & \boldsymbol{B} &= \boldsymbol{b}\, f(t - \boldsymbol{\xi}\cdot\boldsymbol{x}), \end{aligned} \tag{2.2}$$

Substitution of (2.2) into (2.1) leads to

$$\frac{1}{c}\boldsymbol{b} = \frac{\mu}{c}\boldsymbol{h} = \boldsymbol{\xi} \times \boldsymbol{e}, \quad -\frac{1}{c}\boldsymbol{d} = -\frac{\boldsymbol{\epsilon}}{c}\boldsymbol{e} = \boldsymbol{\xi} \times \boldsymbol{h}. \tag{2.3}$$

It easily follows that

$$\boldsymbol{\xi}\times(\boldsymbol{\xi}\times\boldsymbol{e}) = \frac{\mu}{c}\boldsymbol{\xi}\times\boldsymbol{h} = -\boldsymbol{\sigma}\boldsymbol{e}, \tag{2.4}$$

i.e.

$$\boldsymbol{\sigma}\boldsymbol{e} = |\boldsymbol{\xi}|^2\boldsymbol{e} - (\boldsymbol{\xi}\cdot\boldsymbol{e})\boldsymbol{\xi}. \tag{2.5}$$

Then from (2.3)

$$\boldsymbol{h}\cdot\boldsymbol{\xi} = \boldsymbol{b}\cdot\boldsymbol{\xi} = \boldsymbol{d}\cdot\boldsymbol{\xi} = \boldsymbol{e}\cdot\boldsymbol{h} = \boldsymbol{d}\cdot\boldsymbol{h} = 0. \tag{2.6}$$

Also

$$\boldsymbol{\xi}\cdot(\boldsymbol{e} \times \boldsymbol{h}) = -\boldsymbol{e}\cdot(\boldsymbol{\xi} \times \boldsymbol{h}) = \boldsymbol{h}\cdot(\boldsymbol{\xi} \times \boldsymbol{e}) = \frac{1}{c}\boldsymbol{e}\cdot\boldsymbol{d} = \frac{1}{c}\boldsymbol{h}\cdot\boldsymbol{b}. \tag{2.7}$$

We shall often assume that

$$\epsilon_{ij} = \epsilon_i\delta_{ij}, \quad \sigma_{ij} = \sigma_i\delta_{ij}. \tag{2.8}$$

No summation is implied. Then

$$d_k = \epsilon_k e_k, \quad b_k = \mu h_k. \tag{2.9}$$

From (2.7) we have

$$\frac{1}{c}\sum_k \epsilon_k e_k^2 = \frac{1}{c}\mu|\boldsymbol{h}|^2 = \boldsymbol{\xi}\cdot(\boldsymbol{e} \times \boldsymbol{h}). \tag{2.10}$$

From (2.7),(2.8),(2.9) we obtain

$$\frac{\mu\epsilon_k}{c^2}e_k = |\boldsymbol{\xi}|^2 e_k - (\boldsymbol{\xi}\cdot\boldsymbol{e})\xi_k. \tag{2.11}$$

Writing

$$\sigma_k = \frac{\mu\epsilon_k}{c^2} \tag{2.12}$$

and rearranging (2.11) we get

$$e_k = (\boldsymbol{\xi}\cdot\boldsymbol{e})\frac{\xi_k}{|\boldsymbol{\xi}|^2 - \sigma_k}. \tag{2.13}$$

Equation (2.9) for d_k and (2.13) lead to

$$d_k = (\boldsymbol{\xi}\cdot\boldsymbol{e})\frac{\epsilon_k\xi_k}{|\boldsymbol{\xi}|^2 - \sigma_k}. \tag{2.14}$$

Contracting (2.13) with ξ_k, and canceling $\boldsymbol{\xi}\cdot\boldsymbol{e}$ gives

$$\sum_k \frac{\xi_k^2}{|\boldsymbol{\xi}|^2 - \sigma_k} = 1. \tag{2.15}$$

Contracting (2.14) by ξ_k, and using $\boldsymbol{\xi}\cdot\boldsymbol{d} = 0$ we get

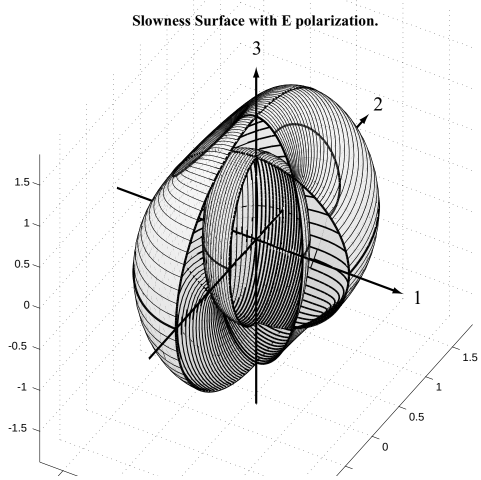

Figure 1: This shows the slowness surface $\mathcal{S}$ cut away to reveal the inner sheet. The contours drawn on the surface are tangent everywhere to the polarization $\boldsymbol{e}$. The thicker contours drawn in each coordinate plane show the circle and ellipse in which that plane cuts the surface. The conical points are clearly visible as the intersections of the ellipse and circle inthe 13-plane. There are also four planes each of which touches $\mathcal{S}$ along a circle. The four circles (only half of one being clearly visible) are drawn as heavy lines surrounding the conical points on the outer sheet.

$$\sum_k \frac{\sigma_k \xi_k^2}{|\boldsymbol{\xi}|^2 - \sigma_k} = 0. \tag{2.16}$$

Equations (2.15) and (2.16) may be taken as equivalent equations of the **slowness surface** $\mathcal{S}_{\boldsymbol{\sigma}}$ on which $\boldsymbol{\xi}$ is constrained to lie. Another equation for $\mathcal{S}$ is

$$\det(\boldsymbol{\sigma} - |\boldsymbol{\xi}|^2 \mathbf{1} + \boldsymbol{\xi}\boldsymbol{\xi}^T) = 0 \tag{2.17}$$

obtained from (2.5) regarded as a linear system in $\boldsymbol{e}$. In (2.17) $\mathbf{1}$ is the identity 3×3 tensor and $\boldsymbol{\xi}^T$ is the transpose of the column vector $\boldsymbol{\xi}$. Equation (2.17) can be written more explicitly as

$$|\boldsymbol{\xi}|^2\, \boldsymbol{\xi}^T \boldsymbol{\sigma} \boldsymbol{\xi} - \mathrm{tr}(\mathrm{adj}\boldsymbol{\sigma})|\boldsymbol{\xi}|^2 + \boldsymbol{\xi}^T \mathrm{adj}\boldsymbol{\sigma}\, \boldsymbol{\xi}] + \det \boldsymbol{\sigma} = 0, \tag{2.18}$$

where adj stands for the transposed matrix of cofactors, and tr for the trace. See Figure 1.

2.2 The wave surface.

Let us now consider the wave surface reciprocal to the slowness surface. Remarkably for the system of crystal optics the algebraic form of the two surfaces is the same.

To see this we first consider the equation of energy conservation

$$\partial_t[\tfrac{1}{8\pi}(\boldsymbol{E} \cdot \boldsymbol{D} + \boldsymbol{H} \cdot \boldsymbol{B})] = -\tfrac{c}{4\pi}\, \boldsymbol{\nabla} \cdot (\boldsymbol{E} \times \boldsymbol{H}). \tag{2.19}$$

This is easily verified from equations (2.1). The quantity $\frac{1}{8\pi}(\boldsymbol{E} \cdot \boldsymbol{D} + \boldsymbol{H} \cdot \boldsymbol{B})$ is the energy density and $\frac{c}{4\pi}\boldsymbol{E} \times \boldsymbol{H}$ is the Poynting vector giving the power flux density. For plane waves $\boldsymbol{E} \cdot \boldsymbol{D} = \boldsymbol{H} \cdot \boldsymbol{B}$, and the Poynting vector is the group, or ray, velocity multiplied by the energy density. It follows by using (2.3) and (2.7) in (2.19) that

$$\tfrac{1}{8\pi}(\boldsymbol{e} \cdot \boldsymbol{d} + \boldsymbol{h} \cdot \boldsymbol{b}) = \tfrac{1}{4\pi}\boldsymbol{e} \cdot \boldsymbol{d} = \tfrac{1}{4\pi}\boldsymbol{h} \cdot \boldsymbol{b} = \tfrac{1}{4\pi}\mu|\boldsymbol{h}|^2 = \tfrac{c}{4\pi}\, \boldsymbol{\xi} \cdot (\boldsymbol{e} \times \boldsymbol{h}). \tag{2.20}$$

from which we may deduce that the ray velocity $\boldsymbol{v}$ is

$$\boldsymbol{v} = \frac{c}{4\pi} \frac{1}{\mu|\boldsymbol{h}|^2} \boldsymbol{e} \times \boldsymbol{h}. \tag{2.21}$$

For future reference let us notice here that from (2.6) and (2.21) the vectors $\boldsymbol{\xi}$, $\boldsymbol{v}$, $\boldsymbol{d}$, and $\boldsymbol{e}$ all lie in the same plane orthogonal to the parallel vectors $\boldsymbol{b}$, $\boldsymbol{h}$.

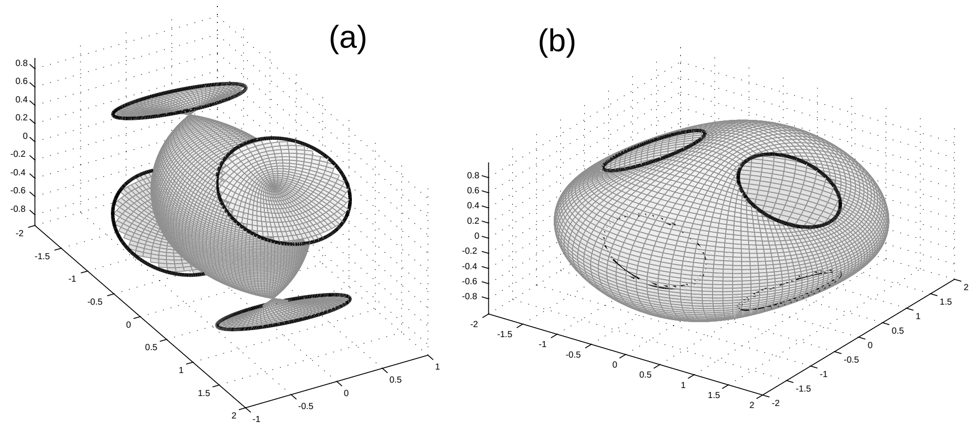

Figure 2: This shows (a) the inner sheet of the wavesurface $\mathcal{W}$ reciprocal to the outer sheet of the slowness surface $\mathcal{S}$ on the left and (b) the outer sheet reciprocal to the inner sheet of the slowness surface on the right. The four prominent 'ears' on the inner sheet have negative Gaussian curvature and correspond to four regions with negative curvature on $\mathcal{S}$. The dark circles are the circles of contact $\mathcal{C}_{\mathcal{W}}$ of the four special tangent planes $\Pi_{\mathcal{W}}$. These circles correspond to conical points on $\mathcal{S}$. Reciprocally the conical points of $\mathcal{W}$ where the 'ears' of the inner sheet meet the 'body' correspond to circles of plane tangency on $\mathcal{S}$. The two sheets join smoothly along the $\mathcal{C}_{\mathcal{W}}$.

From (2.20), (2.21) we have

$$\boldsymbol{\xi} \cdot \boldsymbol{v} = 1. \tag{2.22}$$

We may now verify that

$$\boldsymbol{v} \times (\boldsymbol{v} \times \boldsymbol{d}) \quad = \quad -\sigma^{-1}\,\boldsymbol{d}, \tag{2.23}$$

i.e.

$$\boldsymbol{\sigma}^{-1}\,\boldsymbol{d} = |\boldsymbol{v}|^2\boldsymbol{d} - (\boldsymbol{v}\cdot\boldsymbol{d})\boldsymbol{v}. \tag{2.24}$$

Taking advantage of the fact that $\boldsymbol{\sigma}$ is diagonal in the current coordinate system we may write (2.24) as

$$\frac{1}{\sigma_k}\,d_k = |\boldsymbol{v}|^2 d_k - (\boldsymbol{v}\cdot\boldsymbol{d})v_k, \tag{2.25}$$

leading to

$$\sum_k \frac{v_k^2}{|\boldsymbol{v}|^2 - \dfrac{1}{\sigma_k}} = 1, \qquad \sum_k \frac{\dfrac{1}{\sigma_k}v_k^2}{|\boldsymbol{v}|^2 - \dfrac{1}{\sigma_k}} = 0. \tag{2.26}$$

and

$$\det(\boldsymbol{\sigma}^{-1} - |\boldsymbol{v}|^2\mathbf{1} + \boldsymbol{v}\boldsymbol{v}^T) = 0, \tag{2.27}$$

compare (2.15), (2.16), (2.17). Also

$$|\boldsymbol{v}|^2\,\boldsymbol{v}^T\mathrm{adj}\boldsymbol{\sigma}\,\boldsymbol{v} - [\mathrm{tr}(\boldsymbol{\sigma})|\boldsymbol{v}|^2 - \boldsymbol{v}^T\boldsymbol{\sigma}\,\boldsymbol{v}] + 1 = 0, \tag{2.28}$$

in analogy with the development (2.11) to (2.17). Equations (2.26) and (2.27),(2.28) may be taken as equivalent equations of the **wave surface** $\mathcal{W}_{\boldsymbol{\sigma}}$ upon which $\boldsymbol{v}$ is constrained to lie. See Figure 2. Two double cones $\Sigma_\pm$ having the origin as vertex pass through the circles. Their equations are

$$\chi_\pm(\boldsymbol{\xi}) \equiv (\xi_{c3}x_1 \pm \xi_{c1}x_3)\Big(\frac{\xi_{c3}x_1}{\sigma_1} \pm \frac{\xi_{c1}x_3}{\sigma_3}\Big) + x_2^2 = 0, \tag{2.29}$$

where ξ_{c1}, 0, and ξ_{c3} are the slowness components of the conical point $\boldsymbol{c}_{\mathcal{S}}$.

3 The Cauchy problem

In this section we set up and solve the Cauchy problem for the second-order system of PDE's obtained by eliminating $\boldsymbol{B}$, $\boldsymbol{D}$, $\boldsymbol{H}$ from (2.1). Later we shall evaluate the solution numerically and present some results graphically. Our development is strongly motivated by John (1955), the discussion of the Herglotz-Petrowskii formulae in Gelfand and Shilov (1964), and Petrowskii (1945).

3.1 The second-order equation for $\boldsymbol{E}$

The elimination of $\boldsymbol{B}$, $\boldsymbol{D}$, $\boldsymbol{H}$ from (2.1) yields the single second-order equation

$$\boldsymbol{\sigma}\ddot{\boldsymbol{E}} = -\boldsymbol{\nabla}\times\boldsymbol{\nabla}\times\boldsymbol{E} = (\boldsymbol{\nabla}^2\mathbf{1} - \boldsymbol{\nabla}\boldsymbol{\nabla}^T)\boldsymbol{E}. \tag{3.1}$$

Then, on writing ∂_t for $\partial/\partial t$ (3.1) becomes

$$[\sigma\partial_t^2 - P(\boldsymbol{\nabla})]\boldsymbol{E} = 0, \tag{3.2}$$

where

$$P(\boldsymbol{\xi}) = |\boldsymbol{\xi}|^2\mathbf{1} - \boldsymbol{\xi}\boldsymbol{\xi}^T, \tag{3.3}$$

so that $P(\hat{\boldsymbol{\xi}})$ is the projection onto the plane normal to $\hat{\boldsymbol{\xi}}$. We shall generate the fundamental solution of (3.2) by solving the Cauchy problem for (3.2) in $t > 0$ with initial conditions

$$\boldsymbol{E}(x,0) = 0, \quad \partial_t\boldsymbol{E}(x,0) = \boldsymbol{\sigma}^{-1}\delta(\boldsymbol{x}), \tag{3.4}$$

where

$$\delta(\boldsymbol{x}) = \delta(x_1)\delta(x_2)\delta(x_3). \tag{3.5}$$

By Duhamel's principle this Cauchy problem is equivalent to the inhomogeneous equation

$$[\boldsymbol{\sigma}\partial_t^2 - P(\boldsymbol{\nabla})]\boldsymbol{E} = \mathbf{1}\delta(t)\delta(\boldsymbol{x}), \tag{3.6}$$

with $\boldsymbol{E} = 0$ for $t < 0$. We shall solve this using the following considerations.

3.2 The residue calculation

Let us write

$$L(v,\boldsymbol{\xi}) = v^2\boldsymbol{\sigma} - P(\boldsymbol{\xi}), \tag{3.7}$$

regarding v as a scalar complex variable. Then for large enough $|v|$

$$\begin{aligned} L^{-1}(v,\boldsymbol{\xi}) &= v^{-2}\boldsymbol{\sigma}^{-1}[\mathbf{1} - v^{-2}P(\boldsymbol{\xi})\boldsymbol{\sigma}^{-1}]^{-1} \\ &= v^{-2}\boldsymbol{\sigma}^{-1}\sum_{n=0}^{\infty} v^{-2n}(P(\boldsymbol{\xi})\boldsymbol{\sigma}^{-1})^n. \end{aligned} \tag{3.8}$$

This is a series in inverse even powers of v, starting with v^{-2}. On multiplying this by v^q and integrating around a large circle centered at the origin in the complex v plane we obtain

$$I = \frac{1}{2\pi \mathrm{i}}\oint L^{-1}(v,\boldsymbol{\xi})v^q\,\mathrm{d}v = \begin{cases} 0, & q = 0, \\ \boldsymbol{\sigma}^{-1}, & q = 1. \end{cases} \tag{3.9}$$

Other values of q will not concern us. Let us now evaluate I by residues at the finite poles. When $\xi \neq 0$ there are four simple non-zero poles $\pm V_1$, $\pm V_2$ of L^{-1} and a double pole at $v = 0$. Thus, if we write V_{-1} for $-V_1$ and V_{-2} for $-V_2$, and ∂_v for $\partial/\partial v$ we find on evaluating the residues at the V_N that

$$I = \sum_N \frac{v^q \operatorname{adj} L}{\partial_v \det L}\bigg|_{v=V_N} + \quad \text{residue at } v = 0. \tag{3.10}$$

We may rewrite $\partial_v \det L|_{v=V_N}$ as

$$\begin{aligned} &\partial_v \det L|_{v=V_N} = \partial_v \det(v^2\boldsymbol{\sigma} - P)|_{v=V_N} \\ &\quad = 2V_N \operatorname{tr}(\boldsymbol{\sigma}\operatorname{adj} L). \end{aligned} \tag{3.11}$$

To find the residue at $v = 0$ we expand $(v^2\boldsymbol{\sigma} - P)^{-1}$ in positive powers of v. Thus using

$$\operatorname{adj} P(\boldsymbol{\xi}) = |\boldsymbol{\xi}|^2\boldsymbol{\xi}\boldsymbol{\xi}^T \tag{3.12}$$

we find that

$$\begin{aligned} \det L &= \operatorname{adj}(v^2\boldsymbol{\sigma} - P) \\ &= \operatorname{adj} P + O(|v|^2) \\ &= |\boldsymbol{\xi}|^2\boldsymbol{\xi}\boldsymbol{\xi}^T + O(|v|^2). \end{aligned} \tag{3.13}$$

Recalling that $\det P = 0$ we see that

$$\begin{aligned}\det(v^2\boldsymbol{\sigma} - P) &= v^2\mathrm{tr}(\boldsymbol{\sigma}\mathrm{adj}P) + O(|v|^4) \\ &= v^2|\boldsymbol{\xi}|^2\,\boldsymbol{\xi}^T\boldsymbol{\sigma}\boldsymbol{\xi} + O(|v|^4).\end{aligned} \tag{3.14}$$

So

$$\{\det[L(v,\boldsymbol{\xi}))]\}^{-1} = \frac{v^{-2}}{|\boldsymbol{\xi}|^2\,\boldsymbol{\xi}^T\boldsymbol{\sigma}\boldsymbol{\xi}} + O(1). \tag{3.15}$$

Thus the residue of $v^q L^{-1}$ at 0 is

$$\begin{matrix}\{\text{residue of } v^q L^{-1} \\ \text{at } v = 0\}\end{matrix} = \begin{cases} 0, & q = 0, \\ \dfrac{\boldsymbol{\xi}\boldsymbol{\xi}^T}{\boldsymbol{\xi}^T\boldsymbol{\sigma}\boldsymbol{\xi}}, & q = 1. \end{cases} \tag{3.16}$$

Thus, from (3.9), (3.10), (3.11), and (3.16) we find that

$$\sum_N \frac{\mathrm{adj}L_N}{2V_N\mathrm{tr}(\boldsymbol{\sigma}\mathrm{adj}L_N)} = 0, \tag{3.17}$$

and

$$\sum_N \frac{\mathrm{adj}L_N}{2\,\mathrm{tr}(\boldsymbol{\sigma}\mathrm{adj}L_N)} + \frac{\boldsymbol{\xi}\boldsymbol{\xi}^T}{\boldsymbol{\xi}^T\boldsymbol{\sigma}\boldsymbol{\xi}} = \boldsymbol{\sigma}^{-1}. \tag{3.18}$$

Here we have written L_N for L evaluated at $v = V_N$, $N = \pm 1, \pm 2$.

3.3 The fundamental solution

Let us first seek a matrix plane-wave solution G_ξ of (3.2) in the form

$$G_\xi(\boldsymbol{x},t) = \sum_N \frac{\mathrm{adj}L_N}{2V_N\mathrm{tr}(\boldsymbol{\sigma}\mathrm{adj}L_N)} f(V_N t - \boldsymbol{\xi}\cdot\boldsymbol{x}) \;+ \frac{\boldsymbol{\xi}\boldsymbol{\xi}^T}{\boldsymbol{\xi}^T\boldsymbol{\sigma}\boldsymbol{\xi}} t f'(-\boldsymbol{\xi}\cdot\boldsymbol{x}). \tag{3.19}$$

We first verify that $L(\partial_t, \boldsymbol{\nabla})G_\xi(\boldsymbol{x},t) = 0$. Thus

$$L(\partial_t, \boldsymbol{\nabla})G_\xi(\boldsymbol{x},t) = \sum_N \frac{L_N\mathrm{adj}L_N}{2V_N\mathrm{tr}(\boldsymbol{\sigma}\mathrm{adj}L_N)} f''(V_N t - \boldsymbol{\xi}\cdot\boldsymbol{x}) = \sum_N \frac{\det L_N\,\mathbf{1}}{2V_N\mathrm{tr}(\boldsymbol{\sigma}\mathrm{adj}L_N)} f''(V_N t - \boldsymbol{\xi}\cdot\boldsymbol{x}) = 0, \tag{3.20}$$

since the $\det L_N = 0$. By (3.17) the initial value of G_ξ is

$$G_\xi(\boldsymbol{x},0) = \sum_N \frac{\mathrm{adj}L_N}{2V_N\mathrm{tr}(\boldsymbol{\sigma}\mathrm{adj}L_N)} f(-\boldsymbol{\xi}\cdot\boldsymbol{x}) = 0, \tag{3.21}$$

and by (3.18) the initial value of $\partial_t G_\xi$ is

$$\partial_t G_\xi(\boldsymbol{x},0) = \sum_N \frac{\mathrm{adj}L_N}{2\,\mathrm{tr}(\boldsymbol{\sigma}\mathrm{adj}L_N)} f'(-\boldsymbol{\xi}\cdot\boldsymbol{x}) + \frac{\boldsymbol{\xi}\boldsymbol{\xi}^T}{\boldsymbol{\xi}^T\boldsymbol{\sigma}\boldsymbol{\xi}} f'(-\boldsymbol{\xi}\cdot\boldsymbol{x}) = \boldsymbol{\sigma}^{-1} f'(-\boldsymbol{\xi}\cdot\boldsymbol{x}). \tag{3.22}$$

We are ultimately interested in the matrix point source problem (3.2), (3.4), (3.5) or equivalently (3.6). The link is the plane-wave expansion of the δ-function,

$$\delta(\boldsymbol{x}) = -\frac{1}{8\pi^2}\int_\Omega \delta''(\hat{\boldsymbol{\xi}}\cdot\boldsymbol{x})\,\mathrm{d}\Omega, \tag{3.23}$$

where Ω is the unit sphere $|\boldsymbol{\xi}| = 1$, $\mathrm{d}\Omega$ its surface element, and δ'' is the second derivative of the one-dimensional δ-function. (See John, 1955, Chapter II; Courant and Hilbert, 1962, Chapter VI, Section 11; and Gelfand and Shilov, 1964, Chapter I, Section 3.11.) From (3.21) and (3.22), and setting $f = \delta'$, we see that

$$\begin{aligned} G(\boldsymbol{x},t) &= -\frac{1}{8\pi^2}\int_\Omega G_\xi(\boldsymbol{x},t)\,\mathrm{d}S \\ &= -\frac{1}{8\pi^2}\sum_N \int_\Omega \frac{\mathrm{adj}L_N}{2V_N\mathrm{tr}(\boldsymbol{\sigma}\mathrm{adj}L_N)} \delta'(V_N t - \hat{\boldsymbol{\xi}}\cdot\boldsymbol{x})\,\mathrm{d}\Omega - \frac{t}{8\pi^2}\int_\Omega \frac{\hat{\boldsymbol{\xi}}\hat{\boldsymbol{\xi}}^T}{\hat{\boldsymbol{\xi}}^T\boldsymbol{\sigma}\hat{\boldsymbol{\xi}}}\,\delta''(-\hat{\boldsymbol{\xi}}\cdot\boldsymbol{x})\,\mathrm{d}\Omega. \end{aligned} \tag{3.24}$$

satisfies (3.4) exactly.

3.4 Transformation to an integral over the slowness surface

Here we follow John (1955, Chapter II) and Gelfand and Shilov (1964, Chapter I, Section 6.3). If the wavespeeds $\pm V_N$ are ordered from the most negative to the most positive we find that $V_N(-\boldsymbol{\xi}) = V_{-N}(\boldsymbol{\xi})$. This and the fact that the V_N are homogeneous functions of degree 1 imply that the integral in (3.24) for N is the same as the integral for $-N$. Thus we may combine the terms for $\pm N$ and write

$$G(\boldsymbol{x},t) = -\frac{1}{4\pi^2}\sum_{N=1,2}\int_\Omega \frac{\mathrm{adj}L_N}{2V_N\mathrm{tr}(\boldsymbol{\sigma}\mathrm{adj}L_N)}\delta'(V_N t - \hat{\boldsymbol{\xi}}\cdot\boldsymbol{x})\,\mathrm{d}\Omega - \frac{1}{8\pi^2}\int_\Omega \frac{\hat{\boldsymbol{\xi}}\hat{\boldsymbol{\xi}}^T}{\hat{\boldsymbol{\xi}}^T\boldsymbol{\sigma}\hat{\boldsymbol{\xi}}}t\,\delta''(-\hat{\boldsymbol{\xi}}\cdot\boldsymbol{x})\,\mathrm{d}\Omega. \tag{3.25}$$

In the Nth term of (3.24) let us transform the integral over Ω to one over S_N, $N = 1, 2$. We note that

$$|\boldsymbol{\xi}|^2\,\mathrm{d}\Omega = \cos\theta\,\mathrm{d}S_N = \frac{\boldsymbol{\xi}\cdot\boldsymbol{\nabla}_\xi V_N}{|\boldsymbol{\xi}|\,|\boldsymbol{\nabla}_\xi V_N|}\,\mathrm{d}S_N = \frac{1}{|\boldsymbol{\xi}|\,|\boldsymbol{\nabla}_\xi V_N|}\,\mathrm{d}S_N, \tag{3.26}$$

where $\boldsymbol{\xi} = |\boldsymbol{\xi}|\hat{\boldsymbol{\xi}}$, θ is the angle between $\boldsymbol{\xi}$ and $\hat{\boldsymbol{v}}$ the normal to S_N, and $\mathrm{d}S_N$ is the surface element on S_N and we have used the homogeneity of V_N as a function of $\boldsymbol{\xi}$. We next use the facts that $V_N(\boldsymbol{\xi}) = 1$ on S_N, δ' is homogeneous of degree -2, and that $V_N(\boldsymbol{\xi})$ is homogeneous of degree 1, to get

$$\frac{\delta'(V_N(\hat{\boldsymbol{\xi}})t - \hat{\boldsymbol{\xi}}\cdot\boldsymbol{x})}{V_N(\hat{\boldsymbol{\xi}})} = |\boldsymbol{\xi}|^3\frac{\delta'(V_N(\boldsymbol{\xi})t - \boldsymbol{\xi}\cdot\boldsymbol{x})}{V_N(\boldsymbol{\xi})} = |\boldsymbol{\xi}|^3\delta'(t - \boldsymbol{\xi}\cdot\boldsymbol{x}), \tag{3.27}$$

Finally we write

$$G(\boldsymbol{x},t) = -\frac{1}{8\pi^2}\partial_t\int_{\mathcal{S}} \frac{\mathrm{adj}L(1,\boldsymbol{\xi})\delta(t - \boldsymbol{\xi}\cdot\boldsymbol{x})}{|\boldsymbol{\nabla}_\xi V_N|\,\mathrm{tr}[\boldsymbol{\sigma}\,\mathrm{adj}L(1,\boldsymbol{\xi})]}\,\mathrm{d}S - \frac{t}{8\pi^2}\int_\Omega \frac{\hat{\boldsymbol{\xi}}\hat{\boldsymbol{\xi}}^T\delta''(\hat{\boldsymbol{\xi}}\cdot\boldsymbol{x})}{\hat{\boldsymbol{\xi}}^T\boldsymbol{\sigma}\hat{\boldsymbol{\xi}}}\,\mathrm{d}\Omega, \tag{3.28}$$

where we have combined the two terms $N = 1, 2$ by integrating over the whole of $\mathcal{S}$ which comprises both sheets. Because of the properties of δ the integrals may be written as integrals along curves of intersection of the algebraic surface $\mathcal{S}$ with the plane $\boldsymbol{\xi}\cdot\boldsymbol{x} = t$. We shall elucidate this and make more explicit the various expressions appearing in the integrand.

4 The loop integrals

Consider the integral expression of (3.28) repeated here for convenience

$$G(\boldsymbol{x},t) = -\frac{1}{8\pi^2}\partial_t\int_{\mathcal{S}} \frac{\mathrm{adj}L(1,\boldsymbol{\xi})\delta(t - \boldsymbol{\xi}\cdot\boldsymbol{x})}{|\boldsymbol{\nabla}_\xi v|\,\mathrm{tr}[\boldsymbol{\sigma}\,\mathrm{adj}L(1,\boldsymbol{\xi})]}\,\mathrm{d}S - \frac{t}{8\pi^2}\int_\Omega \frac{\hat{\boldsymbol{\xi}}\hat{\boldsymbol{\xi}}^T\delta''(\hat{\boldsymbol{\xi}}\cdot\boldsymbol{x})}{\hat{\boldsymbol{\xi}}^T\boldsymbol{\sigma}\hat{\boldsymbol{\xi}}}\,\mathrm{d}\Omega. \tag{4.1}$$

The first integral reduces to an integral around a curve, the intersection of $\mathcal{S}$ and the plane $\boldsymbol{\xi}\cdot\boldsymbol{x} = t$. Let $\boldsymbol{n}$ be the outward unit normal to $\mathcal{S}$ and ζ' difined by

$$\zeta' = \hat{\boldsymbol{x}}\cdot\boldsymbol{\xi}. \tag{4.2}$$

Then

$$\sin\theta\,\mathrm{d}\mathcal{S} = \mathrm{d}s\,\mathrm{d}\zeta', \tag{4.3}$$

where s is arclength along the curve and

$$\cos\theta = \hat{\boldsymbol{x}}\cdot\boldsymbol{n} = \frac{\hat{\boldsymbol{x}}\cdot\boldsymbol{\nabla}_\xi v}{|\boldsymbol{\nabla}_\xi v|}. \tag{4.4}$$

Hence

$$\frac{\delta(t - \boldsymbol{\xi}\cdot\boldsymbol{x})\,\mathrm{d}\mathcal{S}}{|\boldsymbol{\nabla}_\xi v|} = \frac{\delta(t - |\boldsymbol{x}|\,\zeta')\,\mathrm{d}s\,\mathrm{d}\zeta'}{\sqrt{|\boldsymbol{\nabla}_\xi v|^2 - (\hat{\boldsymbol{x}}\cdot\boldsymbol{\nabla}_\xi v)^2}}. \tag{4.5}$$

Thus

$$\int_{\mathcal{S}} \frac{\mathrm{adj}L(1,\boldsymbol{\xi})\delta(t - \boldsymbol{\xi}\cdot\boldsymbol{x})}{|\boldsymbol{\nabla}_\xi v|\,\mathrm{tr}[\boldsymbol{\sigma}\,\mathrm{adj}L(1,\boldsymbol{\xi})]}\,\mathrm{d}\mathcal{S} = \frac{1}{|\boldsymbol{x}|}\int_{\mathcal{L}} \frac{\mathrm{adj}L(1,\boldsymbol{\xi})\,\mathrm{d}s}{\mathrm{tr}[\boldsymbol{\sigma}\,\mathrm{adj}L(1,\boldsymbol{\xi})]\sqrt{|\boldsymbol{\nabla}_\xi v|^2 - (\hat{\boldsymbol{x}}\cdot\boldsymbol{\nabla}_\xi v)^2}} \tag{4.6}$$

Here $\mathcal{L}$ is the complete real intersection of $\mathcal{S}$ with the plane $\boldsymbol{\xi}\cdot\boldsymbol{x} = t$ and $\mathrm{d}s$ is arclength along $\mathcal{L}$.

4.1 Implicit computation of the complete intersection $\mathcal{L}$

To evaluate the integral (4.6), we have to compute the complete real intersection $\mathcal{L}$ of $\mathcal{S}$ with the plane $\boldsymbol{\xi}\cdot\boldsymbol{x} = t$. We use an Eulerian approach.

Since

$$\mathcal{S} = \{\xi \in R^3 : \det(\boldsymbol{\sigma} - P(\boldsymbol{\xi})) = 0\}, \tag{4.7}$$

we define the function

$$\Phi(\xi) \equiv \det(\boldsymbol{\sigma} - P(\boldsymbol{\xi})), \tag{4.8}$$

and find its zero level set $\mathcal{S}$:

$$\mathcal{S} = \{\boldsymbol{\xi} \in R^3 : \Phi(\boldsymbol{\xi}) = 0\}, \tag{4.9}$$

Moreover, the hyperplane $\boldsymbol{\xi}\cdot\boldsymbol{x} = t$ may also be represented implicitly by the zero level set of function

$$\Psi(\boldsymbol{\xi}) \equiv \boldsymbol{\xi}\cdot\boldsymbol{x} - t = 0. \tag{4.10}$$

To reduce the computation we use the fact that $\mathcal{L}$ always lies on the plane $\boldsymbol{\xi}\cdot\boldsymbol{x} = t$ with a fixed normal $\hat{\boldsymbol{x}}$. Thus we may rotate the coordinate system first so that $\boldsymbol{\xi}\cdot\hat{\boldsymbol{x}}$ is one of the new coodinates and find $\mathcal{L}$ by contouring zero level sets of a 2-dimensional function of the remaining coordinates. This technique is commonly used in the level set method for dynamic implicit surfaces, see Osher and Fedkiw (2002).

4.2 The method of evaluation

The method of numerical evaluation is as follows. We first rotate the coordinate system so that the new 3-direction is parallel to $\boldsymbol{x}$. Thus, defining the rotation matrix Q to have $\hat{\boldsymbol{x}}$ as its third column (We chose the second column to lie in the 12-plane.), and setting

$$\boldsymbol{\xi} = Q\,\boldsymbol{\xi}' \tag{4.11}$$

the coordinate ξ_3' is in the direction of $\boldsymbol{x}$ as required and ξ_1', ξ_2', ξ_3' form a right-handed orthogonal coordinate system. So, using

$$\boldsymbol{\sigma}' = Q^T\boldsymbol{\sigma}Q, \quad \boldsymbol{\xi}' = Q^T\boldsymbol{\xi} \tag{4.12}$$

we may write the determinant $\det\{\boldsymbol{\sigma} - P(\boldsymbol{\xi})\}$ by (2.18)

$$\det\{\boldsymbol{\sigma} - P(\boldsymbol{\xi})\} = \det\{\boldsymbol{\sigma}' - P(\boldsymbol{\xi}')\} = \sigma_1\sigma_2\sigma_3 - \mathrm{tr}\{\mathrm{adj}(\boldsymbol{\sigma}'\}|\boldsymbol{\xi}'|^2 + \boldsymbol{\xi}'^T\mathrm{adj}(\boldsymbol{\sigma}')\boldsymbol{\xi}' + |\boldsymbol{\xi}'|^2\boldsymbol{\xi}'^T\boldsymbol{\sigma}'\boldsymbol{\xi}' \tag{4.13}$$

as a function of ξ_1' and ξ_2' for each fixed $\xi_3' = t/|\boldsymbol{x}|$. A Matlab code was written using the `contour` command to find $\mathcal{L}$ as a curve or curves of points in the $\xi_1'\xi_2'$-plane where this determinant vanishes. The integration was performed to second order accuracy in the stepsize of the mesh on which $\det\{\boldsymbol{\sigma}' - P(\boldsymbol{\xi}')\}$ was evaluated.

5 The static term

In (3.28) the final term of the fundamental solution G represents a non-propagating disturbance, corresponding to zero velocity, which grows linearly in time and is singular at the origin. It is

$$J(\boldsymbol{x}, t) = -\frac{t}{8\pi^2}\int_\Omega \frac{\hat{\boldsymbol{\xi}}\hat{\boldsymbol{\xi}}^T}{\hat{\boldsymbol{\xi}}^T\boldsymbol{\sigma}\hat{\boldsymbol{\xi}}}\delta''(\hat{\boldsymbol{\xi}}\cdot\boldsymbol{x})\,\mathrm{d}\Omega. \tag{5.1}$$

Let $\hat{x}$ be the unit vector in the direction of $\boldsymbol{x}$ and let $\hat{\boldsymbol{y}}$, $\hat{\boldsymbol{z}}$ be chosen so that $\hat{\boldsymbol{x}}$, $\hat{\boldsymbol{y}}$, $\hat{\boldsymbol{z}}$ form a right-handed orthonormal triple. Then a general unit vector $\hat{\boldsymbol{\xi}}$ perpendicular to $\boldsymbol{x}$ may be written as $\cos\phi\hat{\boldsymbol{y}} + \sin\phi\hat{\boldsymbol{z}}$, and we may write J as

$$J(\boldsymbol{x}, t) = -\frac{t}{8\pi^2|\boldsymbol{x}|^3}\int_{-1}^{1}\int_0^{2\pi} \frac{\hat{\boldsymbol{\xi}}\hat{\boldsymbol{\xi}}^T}{\hat{\boldsymbol{\xi}}^T\boldsymbol{\sigma}\hat{\boldsymbol{\xi}}}\,\delta''(\mu)\,\mathrm{d}\phi\,\mathrm{d}\mu, \tag{5.2}$$

where

$$\hat{\boldsymbol{\xi}} \;=\; \mu\hat{\boldsymbol{x}} + \sqrt{1-\mu^2}(\cos\phi\hat{\boldsymbol{y}} + \sin\phi\hat{\boldsymbol{z}}), \tag{5.3}$$

where $\boldsymbol{x}^\perp = \cos\phi\hat{\boldsymbol{y}} + \sin\phi\hat{\boldsymbol{z}}$. say. Then

$$J(\boldsymbol{x},t) = -\frac{t}{8\pi^2|\boldsymbol{x}|^3}\int_0^{2\pi} \frac{\partial^2}{\partial\mu^2}\left(\frac{\hat{\boldsymbol{\xi}}\hat{\boldsymbol{\xi}}^T}{\hat{\boldsymbol{\xi}}^T\boldsymbol{\sigma}\hat{\boldsymbol{\xi}}}\right)\Bigg|_{\mu=0} \mathrm{d}\phi. \tag{5.4}$$

After some elementary calculations we find that

$$\frac{\partial^2}{\partial\mu^2}\left(\frac{\hat{\boldsymbol{\xi}}\hat{\boldsymbol{\xi}}^T}{\hat{\boldsymbol{\xi}}^T\boldsymbol{\sigma}\hat{\boldsymbol{\xi}}}\right)\Bigg|_{\mu=0} = 2\left[\frac{\hat{\boldsymbol{x}}\hat{\boldsymbol{x}}^T}{{\boldsymbol{x}^\perp}^T\boldsymbol{\sigma}\boldsymbol{x}^\perp} - \frac{2({\boldsymbol{x}^\perp}^T\boldsymbol{\sigma}\hat{\boldsymbol{x}})(\hat{\boldsymbol{x}}{\boldsymbol{x}^\perp}^T + \boldsymbol{x}^\perp\hat{\boldsymbol{x}}^T)}{({\boldsymbol{x}^\perp}^T\boldsymbol{\sigma}\boldsymbol{x}^\perp)^2} + \frac{4(\hat{\boldsymbol{x}}^T\boldsymbol{\sigma}\boldsymbol{x}^\perp)^2\boldsymbol{x}^\perp{\boldsymbol{x}^\perp}^T}{({\boldsymbol{x}^\perp}^T\boldsymbol{\sigma}\boldsymbol{x}^\perp)^3}\right]. \tag{5.5}$$

Thus we need integrals of the form

$$I^{(0)} = \int_0^{2\pi}\frac{\mathrm{d}\phi}{D}, \qquad I^{(2)}_{pq} = \int_0^{2\pi}\frac{x^\perp_p x^\perp_q\,\mathrm{d}\phi}{D^2}, \qquad I^{(4)}_{pqrs} = \int_0^{2\pi}\frac{x^\perp_p x^\perp_q x^\perp_r x^\perp_s\,\mathrm{d}\phi}{D^3}, \tag{5.6}$$

where $D = {\boldsymbol{x}^\perp}^T\boldsymbol{\sigma}\boldsymbol{x}^\perp$ and the superscripts indicate the ranks of the tensors. We begin with $I^{(0)}$ from which the others may be derived by means of

$$I^{(2)}_{pq} = -\frac{\partial I^{(0)}}{\partial\sigma_{pq}}, \quad I^{(4)}_{pqrs} = \frac{1}{2}\frac{\partial^2 I^{(0)}}{\partial\sigma_{pq}\partial\sigma_{rs}}. \tag{5.7}$$

Let us write

$$F = \hat{\boldsymbol{x}}^T\mathrm{adj}\boldsymbol{\sigma}\,\hat{\boldsymbol{x}}. \tag{5.8}$$

Then it may be shown that

$$I^{(0)} = \frac{2\pi}{F^{\frac{1}{2}}}, \tag{5.9}$$

but for want of space we omit the derivation. Let us further define

$$Z_{jk} = \epsilon_{ijk}\hat{x}_i, \quad \mathbf{w} = \boldsymbol{\sigma}\hat{\boldsymbol{x}}, \quad W = Z^T\boldsymbol{\sigma}Z. \tag{5.10}$$

Then, it follows after some further calculation that the static term of (3.28) is given by

$$\begin{aligned}&-\frac{t}{8\pi^2}\int_\Omega \frac{\hat{\boldsymbol{\xi}}\hat{\boldsymbol{\xi}}^T}{\hat{\boldsymbol{\xi}}^T\boldsymbol{\sigma}\hat{\boldsymbol{\xi}}}\,\delta''(\hat{\boldsymbol{\xi}}\cdot\boldsymbol{x})\,\mathrm{d}\Omega = \\ &\quad -\frac{t}{4\pi F^{\frac{1}{2}}|\boldsymbol{x}|^3}\left\{2\hat{\boldsymbol{x}}\hat{\boldsymbol{x}}^T - \frac{\hat{\boldsymbol{x}}^T\boldsymbol{\sigma}\hat{\boldsymbol{x}}}{F}W - \frac{2}{F}(\hat{\boldsymbol{x}}\mathbf{w}^TW + W\mathbf{w}\hat{\boldsymbol{x}}^T) - \frac{2}{F}Z^T\mathbf{w}\mathbf{w}^TZ + \frac{3}{F^2}(\mathbf{w}^TW\mathbf{w})W\right\},\end{aligned} \tag{5.11}$$

with Z, $\mathbf{w}$, and W given by (5.10), and F by (5.8).

We now have the ingredients for evaluating the solution G given in (3.28).

6 The field in the 13-plane

6.1 The 13-section

In this section we plot the solution $G_{ij}(\boldsymbol{x},t)$ as functions of t for various fixed $\boldsymbol{x}$ with $|\boldsymbol{x}| = 1$ and $\boldsymbol{x}$ given by

$$\boldsymbol{x}(\theta) = \begin{pmatrix}\sin\theta\\ 0\\ \cos\theta\end{pmatrix}, \tag{6.1}$$

and $\theta = 0, \pi/36, \pi/18, \ldots, \pi/2$, i.e. θ increasing by steps of 5° from 0° to 90°. This will give a sampling of points on the 13-plane illustrating the various types of behavior in relation to the geometrical configuration described at the end of the previous sections.

Let us first define θ_a, θ_b and θ_c by

$$\tan\theta_a = \sqrt{\frac{\sigma_3(\sigma_1-\sigma_2)}{\sigma_1(\sigma_2-\sigma_3)}}, \quad \tan\theta_b = \sqrt{\frac{\sigma_1(\sigma_1-\sigma_2)}{\sigma_3(\sigma_2-\sigma_3)}}, \quad \tan\theta_c = \sqrt{\frac{\sigma_1-\sigma_2}{\sigma_2-\sigma_3}}. \tag{6.2}$$

Here θ_a and θ_b are the points at which the circle $\mathcal{C}_\mathcal{W}$ crosses the 13-plane, for $\theta = \theta_c$ $\boldsymbol{x}$ is parallel to a biradial and so points in the direction of the conical point $\boldsymbol{c}_\mathcal{W}$. We find that $\theta_a < \theta_c < \theta_b$. See Figure 3 where the 13-section of $\mathcal{W}$ is plotted.

To understand the sequence of arrivals for a given $\boldsymbol{x}(\theta)$ draw the ray through the origin in the direction of $\boldsymbol{x}(\theta)$ in Figure 3. As t increases the point $\boldsymbol{x}(\theta)/t$ will move along the ray through the origin parallel to $\boldsymbol{x}(\theta)$ from outside $\mathcal{W}$ for small t inwards towards the origin. Each crossing of $\mathcal{W}$ is associated with the arrival of a singularity. A normal to $\mathcal{W}$ at one of these crossings gives the direction of the associated stationary point $\boldsymbol{\xi}_{1,2}$ on $\mathcal{S}$. Reciprocally the normal to $\mathcal{S}$ at such a $\boldsymbol{\xi}_{1,2}$ gives the direction of the point $\boldsymbol{x}$ to which it corresponds. Thus at both stationary points $\boldsymbol{\xi}_{1,2}$ corresponding to the ray in the direction of $\hat{\boldsymbol{x}}$, the normals to $\mathcal{S}$ are parallel to $\hat{\boldsymbol{x}}$ and make an angle θ with the 3-axis. The inner sheet of $\mathcal{W}$ corresponds to the outer sheet of $\mathcal{S}$, and vice-versa as indicated in the captions to Figure 2.

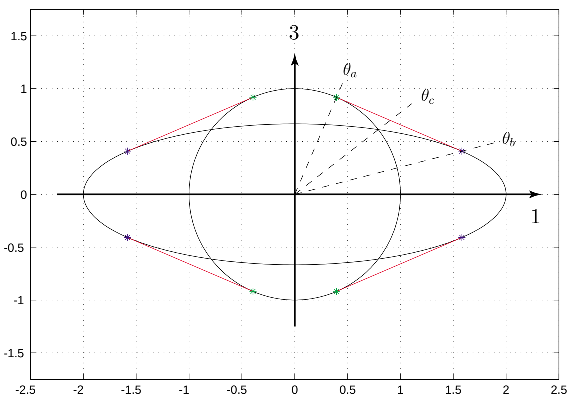

Figure 3: This shows the 13-section of the wave surface $\mathcal{W}$ for fixed time $t = 1$. Notice the ellipse and the circle which intersect at the conical points of $\mathcal{W}$, the biradials, making angle θ_c with the 3-axis. The angles θ_a, θ_b, and θ_c, measured from the 3-axis, are indicated. Notice also the segments of common tangents which represent the disks $\mathcal{D}_\mathcal{W}$ forming a part of the wavefront carrying a weak singularity.

For $0 < \theta < \theta_a$ and again for $\theta_b < \theta < \pi/2$, $\boldsymbol{x}(\theta)$ lies outside the cone Σ_{++} and the singularities all correspond to points of tangency on $\mathcal{S}$ with positive Gaussian curvature. These singularities are of the form

$$\frac{A(\hat{\boldsymbol{x}})\hat{\boldsymbol{e}}_{1,2}\hat{\boldsymbol{e}}_{1,2}^T}{K^{\frac{1}{2}}(\boldsymbol{\xi}_{1,2})|\boldsymbol{x}|}\delta[t - t_{1,2}(\theta)], \tag{6.3}$$

except that a more complicated asymptotic ansatz (not given in this paper) is required for those $\boldsymbol{x}$ having directions passing close to $\theta = \theta_a$ or θ_b, and yet another for θ near θ_c. In (6.3) A is a smoothly varying function of direction, $\boldsymbol{\xi}_{1,2} = \boldsymbol{\xi}_{1,2}(\theta)$ are the two points at which the plane $\boldsymbol{\xi}\cdot\boldsymbol{x}(\theta) = t$ is tangent to $\mathcal{S}$, and $t_{1,2}(\theta)$ the two corresponding values of t, with indexing such that $t_1 < t_2$, and $\boldsymbol{e}_{1,2}(\theta)$ the corresponding polarization for $\boldsymbol{E}$. Then $\boldsymbol{\xi}_1(\theta)$ lies on the inner sheet of $\mathcal{S}$ and $\boldsymbol{\xi}_2(\theta)$ lies on the outer. See Figures 3 & 4. $K(\boldsymbol{\xi}_{1,2}) > 0$ is the Gaussian curvature of $\mathcal{S}$ at $\boldsymbol{\xi}_{1,2}$. See Burridge (1967). For these ranges of directions the plane $\boldsymbol{x}\cdot\boldsymbol{\xi} = t$ passes over $\boldsymbol{c}_\mathcal{S}$ so as to make locally a hyperbolic section with the tangent cone to $\mathcal{S}$ at $\boldsymbol{c}_\mathcal{S}$. There is no corresponding conical wave arrival.

For $\theta = \theta_a$, $\boldsymbol{\xi}_1 = \boldsymbol{c}_\mathcal{S}$ and $\boldsymbol{\xi}_2$ is on the outer sheet still near the 3-axis. In Figures 6 we show the configuration of the loops for θ just less, and just greater than, θ_a. This raises the question of the uniform analytical treatment of the neighborhood of the circle $\mathcal{C}_\mathcal{W}$, the boundary of the disk $\mathcal{D}_\mathcal{W}$. The analysis of this approximation is not known to the present authors for the time-dependent problem, but Borovikov (2000) has recently given a treatment for a closely related time-harmonic case. Afte some preliminary transformation the time-dependent approximation may be derived from this by a Fourier transform, but as far as the authors are aware this has not yet been carried out.

For $\theta_a < \theta < \theta_c$ and for $\theta_c < \theta < \theta_b$ $\chi(\boldsymbol{x}) < 0$ and $\boldsymbol{x}$ lies within the cone Σ_{++}, the Gaussian curvature is negative at the contact point $\boldsymbol{\xi}_1$, which now lies on the outer sheet of $\mathcal{S}$. The wave singularity corresponding to such a point has the form ξ

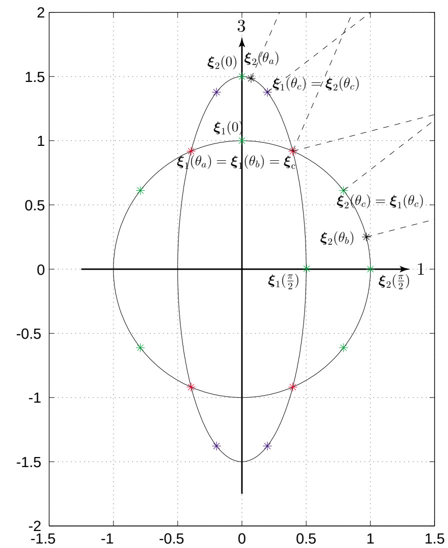

Figure 4: This shows the 13-section of the slowness surface $\mathcal{S}$. Notice the ellipse and the circle which intersect at the conical points of $\mathcal{S}$, the binormals, making angle θ_c with the 3-axis. The points $\boldsymbol{\xi}_{1,2}(\theta)$ are indicated for $\theta = \theta_a, \theta_b, \theta_c$. The normals re in the directions θ_a, θ_b, θ_c.

$$\frac{A(\hat{\boldsymbol{x}})\hat{\boldsymbol{e}}_{1,2}\hat{\boldsymbol{e}}_{1,2}^T}{|K|^{\frac{1}{2}}(\boldsymbol{\xi}_1)|\boldsymbol{x}|}\,\frac{-1}{\pi(t-t_1)}, \tag{6.4}$$

the Hilbert transform of that in (6.3). See Burridge (1967). Notice that for these values of θ this is the first of the two 'geometrical' wave arrivals and it carries a two-sided singularity. Hence the field must already be non-zero. Indeed, when $\chi(\boldsymbol{x}) < 0$ a step singularity arising from the neighborhood of the conical point arrives first, the associated wavefront being the disk spanning a contact circle $\mathcal{C}_{\mathcal{W}}$ on $\mathcal{W}$. See Burridge (1967) for a treatment of the analogous arrival for cubic elastic media when $\boldsymbol{x}$ is not too near the cone Σ_{++}. Notice that the for these $\boldsymbol{x}$ the plane $\boldsymbol{\xi}\boldsymbol{\cdot}\boldsymbol{x} = t$ cuts the cone tangent to $\mathcal{S}$ at $\boldsymbol{c}_{\mathcal{S}}$ in elliptical sections and there is a non-zero conical arrival.

As θ increases from θ_a to θ_c, the stationary point $\boldsymbol{\xi}_1(\theta)$ moves away from the conical point on $\mathcal{S}$ toward the circle $\mathcal{C}_{\mathcal{S}}$ at the lower of $\boldsymbol{\xi}_1(\theta_c) = \boldsymbol{\xi}_1(\theta_c)$, and at the same time the stationary point $\boldsymbol{\xi}_2(\theta)$ moves from $\boldsymbol{\xi}_2(\theta_a)$ outside of the cone Σ_{++} toward the rim of the disk nearest to the 3-axis at the upper point $\boldsymbol{\xi}_1(\theta_c) = \boldsymbol{\xi}_1(\theta_c)$. Both geometrical arrivals come in together at $t = t_1 = t_2$. The direction of $\boldsymbol{x}$ now becomes biradial and passes through the conical point $\boldsymbol{c}_{\mathcal{W}}$ on $\mathcal{W}$. Then all the points of $\mathcal{C}_{\mathcal{S}}$ become stationary points and to find the singularities for directions near biradial one needs to perform a further appropriate uniform asymptotic analysis.

To track these points as θ passes from θ_c to θ_b and in order to keep the order of arrival times so that $t_1 \leq t_2$ the labeling of points must change so that $\boldsymbol{\xi}_1$ becomes $\boldsymbol{\xi}_2$ and vice versa. The old $\boldsymbol{\xi}_2$, renamed as $\boldsymbol{\xi}_1$, now proceeds from the rim to the conical point $\boldsymbol{\xi}_c$ while the old $\boldsymbol{\xi}_1$, renamed as $\boldsymbol{\xi}_2$, proceeds beyond the rim towards the 1-axis, reaching an intermediate position $\boldsymbol{\xi}_2(\theta_b)$ while $\boldsymbol{\xi}_1(\theta_b)$ moves to $\boldsymbol{\xi}_c$.

For θ passing from θ_b to $\pi/2$, $\boldsymbol{\xi}_1$ proceeds on the inner sheet of $\mathcal{S}$ from $\boldsymbol{\xi}_c$ to the direction of the 1-axis and $\boldsymbol{\xi}_2$ also tends to the 1-direction on the outer sheet. In Figure 4 is shown the 13-section of $\mathcal{S}$ with the points $\boldsymbol{\xi}_{1,2}(\theta_{a,b,c})$ indicated. Pairs $\boldsymbol{\xi}_{1,2}$ corresponding to the same θ have parallel normals in the direction of $\boldsymbol{\xi}(\theta)$, making and angle θ with the 3-axis, and indicated as dashed lines in the figure.

6.2 Numerical values of the $G_{ij}(\boldsymbol{x}, t)$ for various $\boldsymbol{x}$ in the 13-plane.

Since the solution is self-similar (homogeneous of degree -2 in $\boldsymbol{x}$ and t) the computation of G was carried out as described above by taking $\boldsymbol{x} = (\sin\theta, 0, \cos\theta)$, for which $|\boldsymbol{x}| = 1$. In Figure 7 the components of G and its time integral are plotted as functions of t for each $\boldsymbol{x}$ corresponding to the values of θ listed above. Let us relate these plots to the geometry of the integration loops. Consider, for instance, the plots in these figures for $\theta = 50°$ and $55°$, close to and on either side of θ_c. See Figure 3. The corresponding integration loops are shown superimposed on the quarter of $\mathcal{S}$ for which $x_1 > 0$ and $x_3 > 0$ in Figure 5.

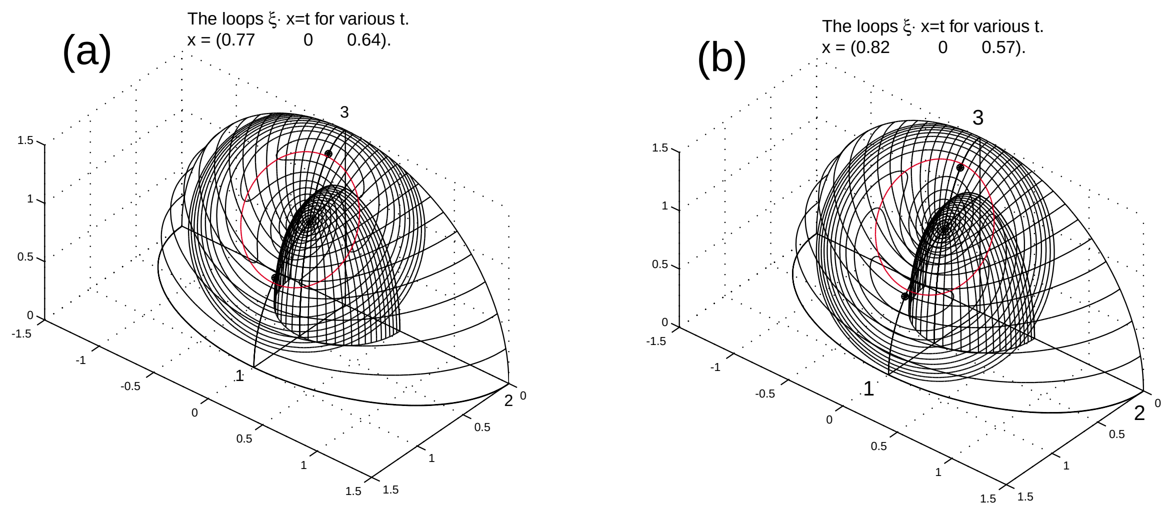

Figure 5: These diagrams show one quarter of $\mathcal{S}$ with integration loops for selected values of t and two positions, $\theta = 50°$ and $55°$, of $\boldsymbol{x}$ on either side of the biradial direction i.e. near the conical point $\boldsymbol{c}_{\mathcal{W}}$ on $\mathcal{W}$. The points marked '⊛' indicate the points of tangency. First the point of negative curvature where the loops are locally hyperbolic and slightly later the point of positive curvature where the lune-shaped loop shrinks to a point.

We may read off the polarization $\boldsymbol{e}_{1,2}$ needed for (6.3) or (6.4) associated with given stationary points ⊛ from the lines marked on $\mathcal{S}$ in Figure 1 and also in Figure 5. We may also approximately read off the amplitude since that is inversely proportional to the square root of the Gaussian curvature of $\mathcal{S}$ at the corresponding stationary point. Notice particularly that the curvature goes to infinity at the conical point, apparently leading to zero amplitude there, but indicating that the waveform has a weaker singularity type. (On the other hand the curvature goes to zero at points of the circles $\mathcal{C}_{\mathcal{W}}$ where the four special tangent planes $\Pi_{\mathcal{S}}$ touch $\mathcal{S}$ indicating a stronger singularity type in the biradial directions.)

The details of the loops in the neighborhood of $\boldsymbol{c}_{\mathcal{S}}$ for an $\boldsymbol{x}$ just outside the cone Σ_{++} are shown in Figure 6(a). For these $\boldsymbol{x}$ there is a stationary point near $\boldsymbol{c}_{\mathcal{S}}$ and marked '⊛', which lies on the inner sheet of $\mathcal{S}$ (as do the other smaller closed loops). The conical point itself is where the loops cross below ⊛. The larger loops, only partially shown in the figure, belong to the outer sheet of $\mathcal{S}$. The time sequence is such that the outer closed loops are paired with the lower open loops at earlier times and a full intersection of $\boldsymbol{\xi}\cdot\boldsymbol{x} = t$ with $\mathcal{S}$ consists of such pairs of loops until the upper ⊛ is reached, when the small closed loops disappear.

The details of the loops for an $\boldsymbol{x}$ just inside the cone Σ_{++} are shown in Figure 6(b). Now the stationary point marked '⊛', which lies on the outer sheet of $\mathcal{S}$. The conical point itself is where the small closed loops (on the inner sheet of $\mathcal{S}$) converge to a point and then open up as closed loops on the outer sheet. The open larger loops belong to the outer sheet of $\mathcal{S}$. The time sequence is that the outer closed loops and the lower open loops are paired at earlier times, and a full intersection of $\boldsymbol{\xi}\cdot\boldsymbol{x} = t$ with $\mathcal{S}$ consists of two loops until ⊛ is reached, when the small closed loops merge with the larger loops to form one large loop like the uppermost (and latest) of the open loops shown.

In Figure 7 are plotted the components of G which are not identically zero by symmetry in the plane $x_2 = 0$ and their time integrals WG. In these figures the $G_{ij}[\boldsymbol{x}(\theta), t]$ are plotted as functions of t for the fixed values of θ indicated on the left vertical scale. The two curves cutting across these indicate the arrival

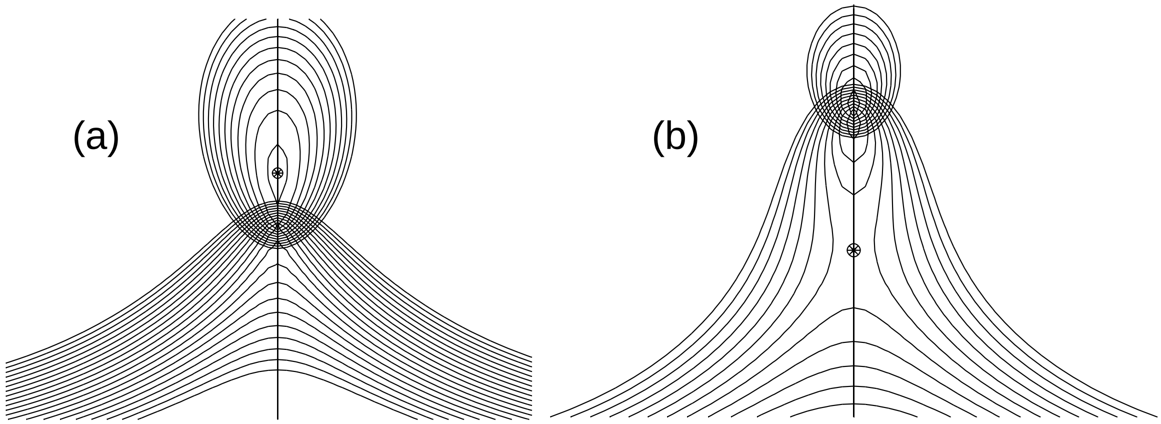

Figure 6: This shows the configurations of loops near the binormal direction, i.e. near the conical point on $\mathcal{S}$, for $\theta = 15°$ (left) and $\theta = 30°$ (right). These directions correspond to points $\boldsymbol{x}$ just just inside and just outside the cone Σ_+. Notice in the left figure the stationary point surrounded by the small loop on the inner sheet of $\mathcal{S}$. The conical point appears where the curves cross. The signal from the conical point is zero in all components. In the right figure the stationary point $\circledast$ is in a neighborhood of negative Gaussian curvature on the outer sheet of $\mathcal{S}$. The local shape of the loops is hyperbolic. The conical point appears where the loops converge above it. $\chi(\boldsymbol{x}) < 0$ here and so $\boldsymbol{x}$ is inside the cone through the circle of tangency $\mathcal{C}_\mathcal{W}$ and there is a nonzero steplike arrival when the loops pass over the conical point. As t increases near these small loops surround the conical point on the inner sheet, shrink to the conical point, and then grow around it on the outer sheet. $\chi(\boldsymbol{x}) > 0$ and so $\boldsymbol{x}$ is (just) outside the cone through the circle of tangency $\mathcal{C}_\mathcal{W}$ and the singularity at $\circledast$ is δ-like, appropriate to positive curvature.

times $t_1(\theta)$ and $t_2(\theta)$. Where these (almost) meet corresponds to θ_c where $t_1 = t_2$. In the plots of each WG_{ij} the horizontal axis is time $t - t_3(\theta)$ after the conical-point arrival. Notice that only in the range $\theta_a < \theta < \theta_b$ (approximately $25° < \theta < 75°$) is the signal non-zero for $t_3 < t < t_1$. In the same range the arrival at t_1 has the Hilbert transform pulse shape. The final arrival, and the leading arrival outside the interval $\theta_a < \theta < \theta_b$, are δ-like for G and step discontinuities for WG.

It is difficult to represent the amplitudes of the δ-like singularities in relation to the smooth parts of the signal, since the amplitudes of the numerical δ's are inversely proportional to the time step and therefore large and dependent upon the discretization. To give a better representation of the singularities in relation to the smooth field we have plotted in the right panels the step response WG_{ij} obtained from the integrals in (3.28) before differentiation with respect to t, plus the time integral of the third term.

7 Conclusions

We have developed the fundamental solution for the time-dependent system of crystal optics using the Herglotz-Petrowskii formula. This technique represents the solution as integrals around real loops, the

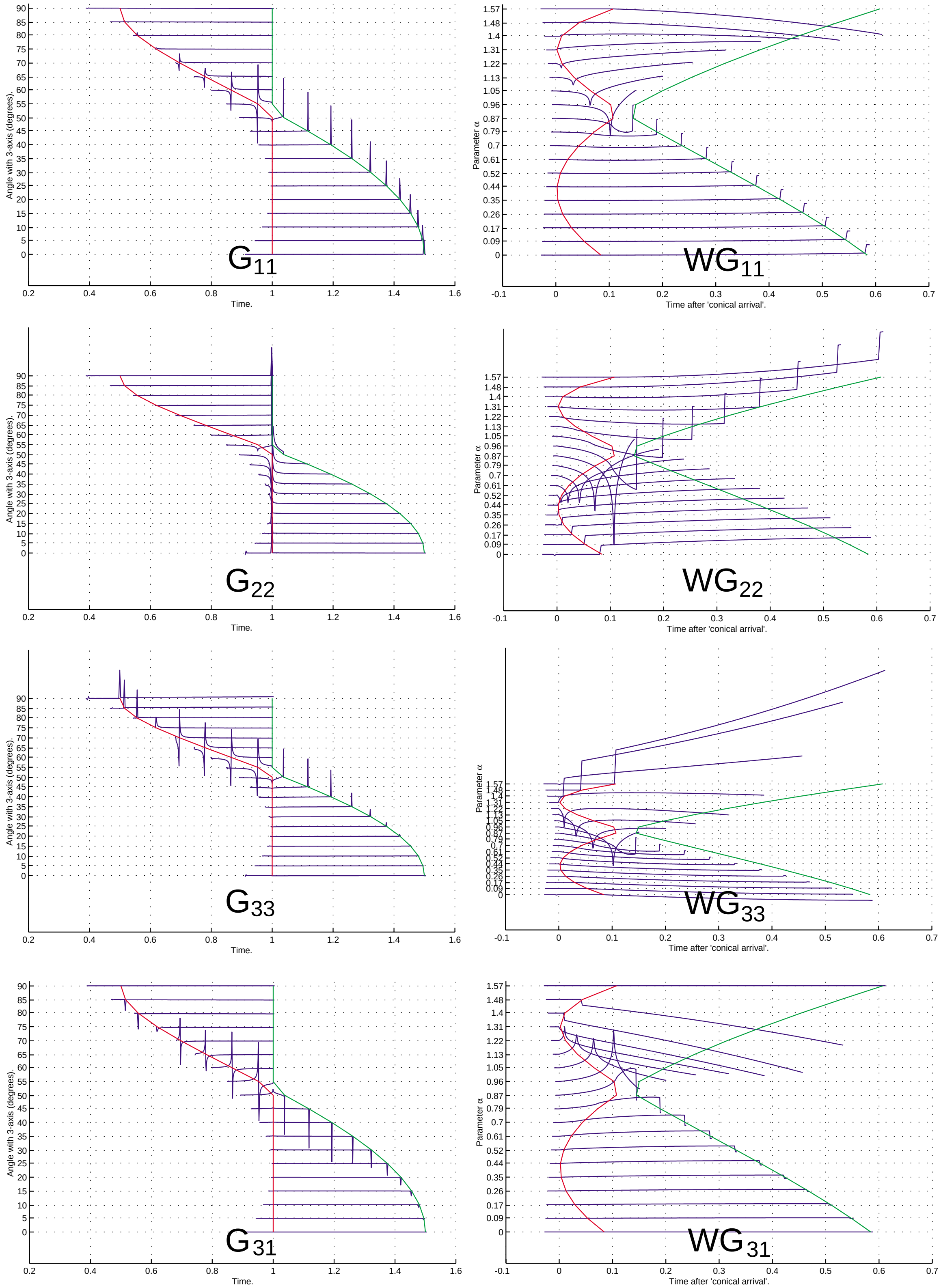

Figure 7: This plots the nonzero components of $G_{ij}(\boldsymbol{x}, t)$ and its time integral $WG_{ij}(\boldsymbol{x}, t)$, the step response, for $\boldsymbol{x}$ having the direction $(\sin\theta, 0, \cos\theta)$ for θ increasing by steps of 5° from 0° to 90°. See the text for further details.

intersection of a moving plane $\boldsymbol{\xi}\cdot\boldsymbol{x} = t$ with the slowness surface $\mathcal{S}$, together with a non-propagating term, which is calculated separately. Because of the identities stemming from the residue calculation of Section 3 and other similar relationships it is possible to express the result in terms of abelian integrals on non-real cycles (Petrowskii, 1945), and possibly a more efficient computation would ensue. These are closely related to the integrals arising in the Cagniard - De Hoop method. See for instance Van der Hijden (1987) for the extension to waves in layered anisotropic elastic media. We have not concerned ourselves with the efficiency of computation, but have used this strikingly geometrical representation to motivate our calculation and to illustrate some special regions of the field, namely the field near the cone of internal conical refraction, and the field near the biradial directions. We found that this representation is easily programmable in Matlab.

We have graphically displayed the geometrical entities that come into play and plotted the signal $G(\boldsymbol{x}, t)$ as functions of t for linear 'gathers' of positions $\boldsymbol{x}$ in the style used in seismic exploration. Since it is not straightforward to represent graphically the amplitude of the Dirac δ we have in one or two places plotted the step response. It is an easy matter to calculate the field to any degree of accuracy in any region using our method. The same method may be used for the fundamental solution for infinitesimal anisotropic elasticity.

We have left for future study the analysis of the uniform asymptotics for field points near the the biradial directions associated with the conical points $\boldsymbol{c}_{\mathcal{W}}$ on the wavesurface $\mathcal{W}$ and near (the surfaces of) the cones of internal conical refraction $\Sigma_{\pm}$. We note that Borovikov has obtained related time-harmonic results where the cone is strictly conical in that it has straight generators but with a nonlinear phase function.

Acknowledgment

The authors wish to thank the Institute for Mathematics and its Applications, University of Minnesota, Minneapolis, and its staff, for giving them the opportunity and encouragement to begin this project there during the first six months of 2002.

References

1. Al'shits, V.I. and J. Lothe, Elastic waves in triclinic crystals. I. General theory and the degeneracy problem, Sov. Phys. Crystallogr. **24**, (1979a), 387-392, (Kristallografiya, **24**, (1978), 672-682.)

2. Al'shits, V.I. and J. Lothe, Elastic waves in triclinic crystals. II. Topology of polarization fields and some general theorems, Sov. Phys. Crystallogr. **24**, (1979b), 393-398, (Kristallografiya, **24**, (1979), 683-693.)

3. Al'shits, V.I. and J. Lothe, Elastic waves in triclinic crystals. III. The problem of existence of exceptional surface waves and some of their general properties, Sov. Phys. Crystallogr. **24**, (1979c), 644-648, (Kristallografiya, **24**, (1979), 1122-1130.)

4. Atiyah, M.F., R. Bott, and L. Garding, Lacunas for hyperbolic differential operators with constant coefficients I & II, *Acta Mathematica,* **124**, (1970), 109-189, and *Acta Mathematica,* **131**, (1973), 145-205.

5. Born, M. and E. Wolf, *Principles of Optics*, Sixth (Corrected) Edition, Pergamon Press, New York, (1989).

6. Borovikov, V.A., The Stationary Phase Method for Surfaces with Conical Points, Russ. J. Math. Phys. **7**, (2000), p. 147.

7. Burridge, R., The singularities on the plane lids of the wave surface of elastic media with cubic symmetry, Quart. J. Mech. and App. Math. **XX**, (1967), 41-55.

8. Burridge, R., Asymptotic evaluation of integrals related to time-dependent fields near caustics, *SIAM J. App. Math.* **55**, (1995), 390-409.

9. Courant, R. and D. Hilbert, *Methods of Mathematical Physics, Vol. II*, Interscience, New York, (1962).

10. Every, A.G., Ballistic phonons and the shape of the ray surface in cubic crystals, *Phys. Rev. B* **24**, (1981), 3456-3467.

11. Fresnel, A.J., *Mémoires do l'Institut,* **VII**, (1827), 136.

12. Gel'fand, I.M. and G.E. Shilov, *Generalized Functions, Vol. I*, Academic Press, (1964).

13. Hamilton, W.R., Trans. Roy. Irish Acad. **17**, (1833), 1.

14. Van der Hijden, J.M.T., *Propagation of Transient Elastic Waves in Stratified Anisotropic Media*, North-Holland, Amsterdam, (1987).

15. John, F., *Plane Waves and Spherical Means*, Interscience, New York, (1955).

16. Lloyd, H., Trans. Roy. Irish Acad. **17**, (1833), 145.

17. Movskin, D.N., V.P. Romanov and A.Y. Val'kov, *Phys. Rev. E* **48**, (1993), 1436.

18. Osher S. J. and R. P. Fedkiw, *The level set method and dynamic implicit surfaces*, Springer-Verlag, New York, (2002).

19. Petrovskii, I.G., On the diffusion of waves and lacunas for hyperbolic equations, *Mat. Sbornik* **17**, (1945), 289-270.

20. Salmon, G., *Analytical geometry of Three Dimensions*, Revised by R.A.P. Rogers, Vol. 2, Longmans, Green & Co., (1915).

21. Shuvalov, A.L. and A.G. Every, Curvature of acoustic slowness surface of anisotropic solids near symmetry axes, *Phys. Rev.* **B53**, (1996), 14906.

22. Smit, D. and M.V. de Hoop, The geometry of the hyperbolic system for an anisotropic perfectly elastic medium, *Comm. Math. Phys.* **167** (1995) 255-300.

23. Warnick, K.F. and D.V. Arnold, Secondary dark rings of internal conical refraction, *Phys. Rev. E* **55**, (1997), 6092-6096.